

Cross-beta structure of an amyloid-forming peptide studied by electron nano-crystallography

Ruben Diaz-Avalos*, Chris Long, Eric Fontano, Melinda Balbirnie, Robert Grothe, David Eisenberg and Donald L.D. Caspar

Institute of Molecular Biophysics, Florida State University, Tallahassee, FL 32306.

*Corresponding Author: Ruben Diaz-Avalos,

Fibre Diffraction Review **11**, 79-86, 2003

ABSTRACT

The seven residue peptide GNNQQNY from the N-terminal region of the yeast prion protein Sup35, which forms both amyloid fibres and highly ordered microcrystals, provides a model system for characterizing the structure and stability of the elusive cross-beta amyloid conformation. Microcrystals of this peptide, which have largest dimension $\sim 1\mu\text{m}$ in the cross-beta fibre axis direction, diffract electrons to ultra high resolution ($<0.5\text{\AA}$ spacing). The sharp 4.86\AA layer-line spacing (with no trace of a 9.72\AA spacing) establishes that the peptide chains form parallel β -sheets. The space group is $P2_12_12_1$ with cell dimensions ranging from $|a| = 22.7\text{-}21.2$, $|b| = 39.9\text{-}39.3$, $|c| = 4.89\text{-}4.86\text{\AA}$ for the wet to dried state. The relative intensities of the Bragg reflections determined from the electron diffraction data indicate that the backbones of the four peptides in the unit cell are aligned closely parallel to the a-axis, with the cross-beta sheets connected in two pairs related by the crystal 2-fold screw axes. Comparison of the cell volume with that calculated for the four peptides implies that water may occupy only 10-15% of the volume in the hydrated state. This nearly anhydrous packing can account for the insolubility of the crystalline aggregates of this hydrophilic peptide, since the activation energy for rehydration may be extremely high. Water excluding packing of paired cross- β peptide segments in thin protofilaments may be a general characteristic of the wide variety of anomalously stable pathological amyloid assemblies.

Introduction

The cross- β polypeptide conformation is characteristic of the pathological amyloid fibre aggregates associated with various neuro-degenerative diseases, including Alzheimer's, Huntington's and Parkinson's, as well as systemic amyloidoses. This fibrous protein folding, in which the β -strand direction is nearly perpendicular to the fibre axis, was first identified by X-ray diffraction from oriented specimens of denatured globular (Astbury, 1935) and fibrous (Rudall, 1952) proteins. In contrast to the familiar fibrous proteins consisting of extended α -helices (eg, keratin, myosin and fibrin), collagen triple helices or β -strands (e.g. silks), the cross- β conformation is rare among naturally occurring biological fibres (Fraser and MacRae, 1973). Cross- β appears to be a dead-end for protein folding. Exceptionally rare, protease-resistant, fibrous amyloid aggregates can be formed by proteins and peptides with uncorrelated amino-

acid compositions and sequences by self-nucleated self-assembly. Beyond the evident regularly periodic cross- β sheet hydrogen bonding in the fibre axis direction, there is little experimental data regarding the atomic structure of amyloid aggregates that can account for their pathological stability and self propagating properties.

The cross- β structure was not fully characterized until the late 1960's, in the work of Eanes and Glenner (1968) and Bonnar *et al.* (1969) from X-ray patterns of partially-aligned specimens taken from human patients afflicted with amyloidosis. The characteristic signature of the cross- β fibre diffraction pattern is a sharp $4.7 - 4.9\text{\AA}$ meridional maximum, accompanied by a $\sim 10\text{\AA}$ equatorial reflection, indicative of a β -sheet structure oriented with the polypeptide chains perpendicular to the fibre axis. The absence of a $\sim 9.6\text{\AA}$ layer-line spacing in the diffraction patterns of most amyloids indicates a tendency to a parallel β -sheet structure.

However, due to the disorder in these specimens, an anti-parallel structure cannot be excluded.

Synthetic peptides corresponding to some portions of amyloidogenic proteins assemble into fibres with all the amyloid characteristics (Kirschner *et al.*, 1987). In particular, peptides from the Alzheimer's amyloid A β -protein form cross- β fibrils, but different fragments have shown both parallel (Benzinger *et al.*, 1998) and anti-parallel β -sheet structure (Halverson *et al.*, 1990; Serpell and Smith, 2000). The presumption is then that the Ab amyloid fibrils may contain both parallel and anti-parallel β -sheets.

The best characterized cross- β structure is the egg-stalk of the green lace-wing fly, *Chrysopa flava*. The X-ray fibre pattern (Geddes *et al.*, 1968) clearly shows the 9.48Å spacing diagnostic of the anti-parallel β -sheet, but diffraction on this layer-line is weak compared to the 4.74Å layer-line marking the hydrogen-bonded chain separation. An atomic model for the peptide backbone was constructed, but unlike the detailed fibre patterns obtained from TMV and filamentous phage, the *Chrysopa* silk pattern does not provide sufficient information to define the atomic structure. It is evident that even with some simple amyloid-forming peptides, using a variety of biophysical tools, it is proving difficult to obtain detailed information about the cross- β atomic structure that can be related to biologically critical properties of amyloid.

The synthetic heptapeptide GNNQQNY from the prion determinant sequence of the yeast Sup35 protein forms a gel that shows all the characteristics of amyloid aggregates, and crystallizes spontaneously in aqueous solutions (Balbirnie *et al.*, 2001). No conditions have been found to dissolve these crystals in the presence of water.

Materials and Methods

Peptide synthesis and crystallization. The peptide (Gly-Asn-Asn-Gln-Gln-Asn-Tyr) has been synthesized at the Chemistry Department of Florida State University and at the Biopolymer Synthesis Center of the California Institute of Technology using F-moc and T-boc chemistry respectively. The peptide was then purified by reverse phase chromatography, dissolving the peptide in 8M Guanidine Hydrochloride, and eluting with a 0-70% acetonitrile gradient. The fractions containing the peptide were immediately dipped in liquid Nitrogen

and lyophilized. The purity of the powder was assessed by mass spectrometry to be greater than 98%, and sequencing of the peptide showed it to have the correct amino-acid composition. A sample of the lyophilized peptide was put in an X-ray beam in order to make sure that aggregation had not occurred up to this point. Suspensions containing microcrystals were prepared as described in Balbirnie *et al.* (2001); solubilization of the peptide in water to a final concentration about 50mg/ml produced a thick gel which showed the characteristic green birefringence of an amyloid aggregate complexed with Congo red when viewed between crossed polarizers.

X-ray powder diffraction. Samples for X-ray powder diffraction were prepared under different solvent conditions by placing a small drop of crystal suspension on a quartz capillary, and centrifuging the capillary softly to sediment the crystals to the bottom. After collecting an X-ray pattern at room temperature, a cold nitrogen stream was used to lower the temperature of the sample to ~100K, and another diffraction pattern collected. The sample was then brought to room temperature and the excess water removed. Pure ethanol was then added to the capillary and the suspension stirred, after which the sample was centrifuged and the supernatant (ethanol) removed. The process was repeated once, and the sample placed in the X-ray beam to collect powder diffraction data at room and liquid nitrogen temperatures. The same process was repeated to replace the ethanol with acetone.

In order to test the effects of drying on the microcrystals, another sample of the crystalline suspension was placed in an evacuated dessicator containing P₂O₅ for three days in order to emulate the conditions found in the column of the electron microscope, and X-ray diffraction patterns were collected at room and liquid nitrogen temperatures. The X-ray powder patterns were collected with a Rigaku generator, using a copper anode and recorded with either an R-axisII image plate detector or a MAR research CCD detector.

Electron diffraction. A 4 μ l drop of sample (1:4 crystal suspension) was placed on a copper grid with a continuous carbon film for about two minutes. The excess solution was then blotted and a drop (4 μ l) of 1% (w/v) dextrose applied to the grid and blotted immediately. The grid was then left to dry for about 10 minutes before inserting into the microscope. In

order to have an internal calibration standard, we used evaporated gold on some samples. However, the inclusion of evaporated metals in the support film was somewhat disruptive for the data collection, with the least disruptive combination being a sandwich of gold between two carbon layers.

The samples were placed in a cryo-holder and inserted into the column of the microscope, where they were observed at liquid Nitrogen temperature. The crystals used for electron diffraction data collection were elongated, with dimensions the order of $1\mu\text{m}$ in length, and about 1000\AA in width and thickness. The electron diffraction patterns were collected using a slightly convergent beam to confine the irradiated area to a region not much larger than the crystal, and the diffracted area was further reduced with a selected area aperture to $\sim 1000\text{\AA}$ in diameter. Once a crystal was found, a diffraction pattern was collected, and if this pattern was seen to arise from a single crystal with no obvious mosaic spread, a tilt series was collected from it, with the number of patterns recorded being constrained mainly by radiation damage. A diffraction pattern was collected at 0° at the end of the process, to assess the radiation damage inflicted on the sample. Some of the tilt series were collected using small angular increments in order to determine the shape of the Bragg reflections, as well as the mosaicity of the crystals.

The electron diffraction data was initially collected on Kodak SO163 film plates with a Philips CM30FEG microscope using an accelerating voltage of 300kV, and later on a JEOL 400 microscope fitted with a 2048 x 2048 pixel slow scan CCD camera (Gatan, Inc.) at the Lawrence-Berkeley laboratory, using an accelerating voltage of 400kV. The camera length values used for the data collection were between 1 and 2.5m.

Indexing of the electron diffraction data. The electron diffraction data was converted to R-axis format in order to use software readily available for X-ray crystallography, such as Denzo (Otwinowski and Minor, 1996) and MOSFLM (Leslie, 1999). However, the autoindexing algorithms of these programs do not take into account the finite size of the Bragg reflections and produced inconsistent results. We attempted then to index the data simulating the shape of the spots to be ellipsoidal (Dimmeler and Schroeder, 2000), but found the simulations to be unsatisfactory. The data were

indexed by hand, using at first the unit cell dimensions determined from the X-ray powder patterns. The use of these values produced systematic deviations in the indexing that were easily corrected by modifying the unit cell parameters slightly to make all the data self-consistent. In some of the tilt series, the presence of either \mathbf{a}^* or \mathbf{b}^* was evident, allowing us to determine directly the ratio of either $\mathbf{a}^*/\mathbf{c}^*$ or $\mathbf{b}^*/\mathbf{c}^*$ for that series, and given that \mathbf{c}^* shows little variation between the wet and the dried state, we were able to find accurate values for \mathbf{a}^* and \mathbf{b}^* .

Profile of the Bragg reflections. In order to determine the profile of the Bragg reflections, we needed to map the intensities of some reflections in the direction of the beam. To this end, it is necessary to determine the orientation of the reciprocal lattice with respect to the Ewald sphere. When successive frames of a tilt series differ by a sufficiently small angle, a given reflection appears in several frames. This permits an accurate estimation of the tilt angle that would give the maximum intensity of that reflection. Since the positions in reciprocal space of the reflections are known, we are able to determine the orientation with which the Ewald sphere samples reciprocal space in each frame.

Processing of the X-ray powder diffraction patterns The powder diffraction patterns were converted to raw images, and centred by minimizing the difference between the diffraction pattern with its own image, rotated by 180° . The centred pattern was then converted to polar coordinates and the image collapsed in the azimuthal direction to produce an average radial profile, which was corrected for the effects of the sphere of reflection in order to convert the data from detector to reciprocal space. The patterns were indexed on a 2-dimensional lattice using the reflections corresponding to spatial frequencies lower than $\sim 5\text{\AA}$, which belong to the $hk0$ plane, and then adding the appropriate \mathbf{c} -dimension to account for all the observed reflections.

Results

Crystal morphology The peptide micro-crystals imaged in the electron microscope do not have the smooth appearance of a single crystal, but they always have striations running along their long axis (Fig. 1). The long axis has the $\sim 4.8\text{\AA}$ periodicity

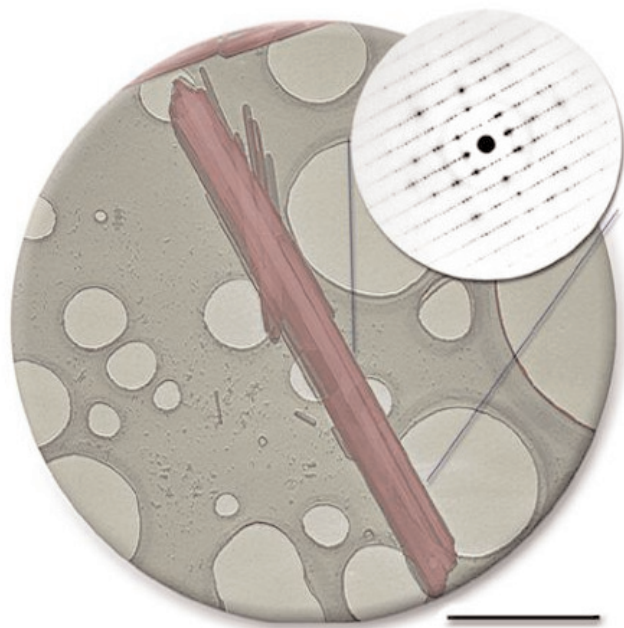


Figure 1. False colour electron micrograph of a peptide crystal, imaged over perforated carbon. The bar indicates 0.5 μm . Some smaller crystals can be observed in the background. The long dimension of the crystal is the c-axis, which has a repeat distance of 4.86 \AA , corresponding to the hydrogen bonding between β -sheets. The inset shows the electron diffraction pattern of the indicated region.

typical of hydrogen bonding corresponding to a parallel β -sheet structure. The presence of Bragg reflections at high angles (corresponding to Bragg spacings of $1/(0.8\text{\AA})$ in Fig. 2A and $(1/0.5\text{\AA})$ in Fig. 2D) indicates a high degree of order in the crystals. Smaller crystals with widths the order of 300 \AA can be easily found in the samples, which is consistent with the half-width measured from the reflections in the powder patterns collected at the synchrotron (Balbirnie *et al.*, 2001). On occasion, we have

found crystals that yield diffraction patterns showing a continuous or nearly continuous intensity distribution along layer-lines, but with strong equatorial sampling (Fig.2C), suggestive of colloidal columnar crystalline ordering.

We collected in excess of 500 electron diffraction patterns from single crystals on film plates, and ten tilt series with the CCD camera at the Lawrence-Berkeley Laboratory, comprising a total of 280 diffraction patterns. Since the crystals lie on the grid with their long axes in the plane of the carbon film, but with these axes randomly oriented relative to the fixed tilt axis of the microscope, each tilt series samples a different region of the reciprocal lattice. Comparison of the diffraction patterns at the start and at the end of the tilt series shows the radiation damage to be noticeable after recording about 25-30 diffraction patterns, although we were able to collect up to ~ 45 patterns from a single crystal.

Unit cell dimensions The crystals always produced diffraction patterns (with X-rays and electrons) that can be indexed with an orthorhombic unit cell. From the X-ray powder patterns we found that the unit cell dimensions change slightly as a function of the solvent bathing the crystals, as summarized in Table 1. Axes **b** and **c** show little variability, while the **a** axis shows a variation the order of 1.4 \AA ($\sim 6\%$) at room temperature, and 0.92 \AA ($\sim 4\%$) at $\sim 100\text{K}$. The electron diffraction data show an even greater degree of variability. From the electron diffraction data collected at Berkeley, we measure $|\mathbf{a}| \sim 22.2\text{\AA}$. However, precise measurements that we have carried out with

Table 1. Unit cell values under different environmental conditions

Temperature ($^{\circ}\text{K}$)	Solvent	a(\AA)	b(\AA)	c(\AA)	V(\AA^3)
300 X-rays	acetone	23.06	39.94	4.87	4490
	ethanol	22.98	39.88	4.89	4479
	water	22.93	39.95	4.89	4480
	dried	21.65	39.84	4.86	4192
100 X-rays	water + cryo-protectant \ddagger	22.6	39.4	4.88§	4345
	ethanol	21.97	39.95	4.88	4283
	water	22.69	39.68	4.87	4384
	dried	21.78	39.29	4.86	4159
EM	glucose (slow frozen)	21.2 \pm 0.2	39.4 \pm 0.24	4.87 \pm 0.02	4068 \pm 78
	glucose	21.8 \pm 0.3	39.4 \pm 0.3	4.87	4189
	glucose (fast frozen)	22.7 \pm 0.2	39.4 \pm 0.3	4.88 \pm 0.02	4353

§Indexing the strongest reflection as 021

\ddagger Balbirnie *et al.*, 2001

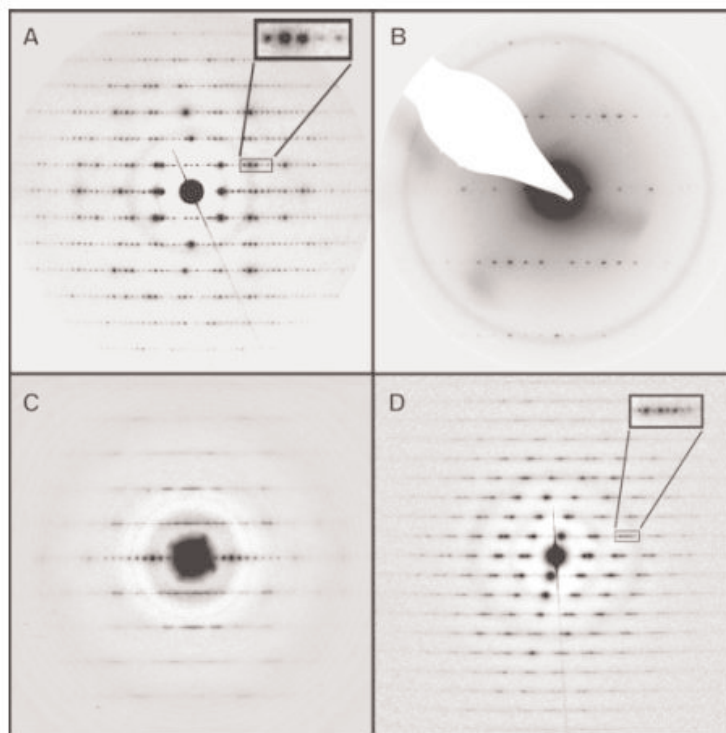


Figure 2. Gallery of electron diffraction patterns of the GNNQQNY peptide (the patterns are reproduced on different scales to illustrate particular features). The absence of any trace of a 9.4\AA axial spacing unambiguously rules out the possibility of an anti-parallel β -sheet structure in the crystals. (A) Typical electron diffraction pattern of a microcrystal. (B) Pattern of a crystal with the incident beam oriented very nearly along the **b**-axis, showing the systematic absence of reflections in the **a** and **c**-axes. The faint ring near the second layer-plane is due to evaporated gold, used as a calibration standard. (C) Pattern showing fibre-like (continuous transform) layer-lines. (D) ED pattern showing reflections extending to the 9th layer-line with $(1/0.53\text{\AA}^{-1})$ Bragg spacing. The patterns shown in (A) and (D) were collected at the Lawrence-Berkeley Laboratory, while those shown in (B) and (C) were collected at FSU. The insets in (A) and (D) show the separation of the Bragg reflections.

evaporated gold included with the specimen have yielded values of $|a|$ between 21.2 and 22.7\AA . The difference in these measurements arises from the procedure followed for the data collection. The samples that gave the lower value for the **a** axis were inserted into the microscope column at room temperature, and cooled after they had been in the ultra high vacuum for a few minutes, whereas the samples that gave the larger value for the **a** axis were frozen to liquid Nitrogen temperature before being inserted into the microscope, and therefore retained more moisture. Thus the indication is that the spacing corresponding to the **a**-axis is related to the water activity.

Crystallographic space group The systematic absence of odd reflections in the $h00$, $0k0$ and $00l$ directions (Fig. 2B) indicates that the crystals have $P2_12_12_1$ symmetry. This implies that there are $4n$ monomers in the unit cell, and from volume and density considerations it is found that $n=1$ (Balbirnie *et al.*, 2001).

Shape of the Bragg reflections Analysis of the

widths at half-maximum of the powder diffraction patterns collected at the synchrotron suggests a domain size the order of 300\AA for the crystals that give rise to the pattern, consistent with the dimensions of the smaller crystals observed in electron micrographs. The determination of the width of the Bragg reflections in electron diffraction patterns is complicated by the fact that the relatively high energy of the 400 keV electrons produces a considerable amount of secondary electrons in the scintillator of the detector being used, blurring each Bragg reflection into several neighbouring pixels. However, the profile of the Bragg reflections in the direction of the beam was carefully determined for one series in which the angular step was small (1°), and we found it to be the order of $1/120\text{\AA}^{-1}$. The fact that spots of comparable intensity (but different spacings) remain in reflecting position throughout the same number of frames indicates that the extent of the reflections increases as a function of the distance from the c^* axis (Fig. 3).

Discussion

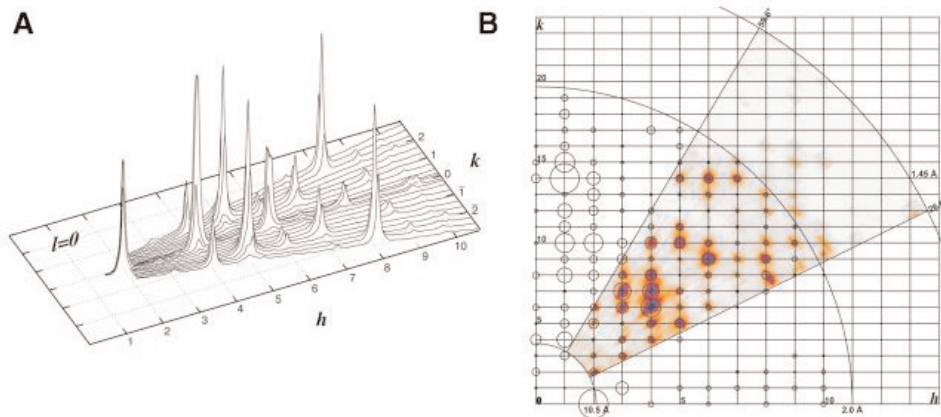


Figure 3. (A) Plot of the observed equatorial intensities throughout a tilt series that included the \mathbf{a}^* axis. The angular increment between frames was 1° , which amounted to $\sim 0.73^\circ$ in the equatorial plane. The spots show a considerable spread in reciprocal space. (B) Image of the intensities in a section of the $HK0$ plane, coloured according to the intensity. The circles at the reciprocal space locations have a diameter proportional to the intensity. This plot shows spots with an angular spread that increases with the distance from the origin.

Electron micrographs of the frozen hydrated suspension of crystals show that fibrils and thin sheets of peptide can coexist with the microcrystals (data not shown). The thin sheets have a variable width, and are long, with a morphology reminiscent of the larger microcrystals, only much thinner. Our attempts at collecting electron diffraction or high resolution images from these sheets have been unsuccessful so far. However, we have seen that these thin sheets tend to curl up or twist, giving the impression of fibrils that would have the characteristic signature of amyloids.

Some of the electron diffraction patterns show a colloidal crystalline character (Fig. 2C). The separation between the equatorial reflections in this pattern corresponds to a real space distance of 21.3 \AA , which is in the lower end of the length measured for the \mathbf{a} -axis, but slightly larger than the width of a pair of β -sheets, which in the case of this peptide is $\sim 19.7 \text{ \AA}$. This columnar crystalline pattern could arise from a regular lateral packing of protofilaments consisting of twisted paired cross- β sheets that are randomly rotated or axially translated relative to each other.

The presence of $\mathbf{P2}_1\mathbf{2}_1\mathbf{2}_1$ symmetry in the crystals imposes stringent constraints on the packing of the peptide in the unit cell. However, there is still some ambiguity to be resolved before producing a final atomic model for the crystal. At this point we favor a model that has four molecules per unit cell (Fig. 4), with the tyrosine rings face-to-face, related by a 2-fold screw axis. The peptide in this model has the

backbone nearly along the \mathbf{a} -axis, and the N-terminus located near the point $(a/4, b/8, c/4)$. There must be a slight tilt of the backbone with respect to the \mathbf{a} -axis ($\sim 7^\circ$), so as to weaken the intensities along the \mathbf{b} -axis, while producing a strong $(1,14,0)$ reflection. The side chains are nearly parallel to the \mathbf{ab} -plane. The strong peak observed at 9.85 \AA in the X-ray powder patterns of the wet samples can be indexed as 220 and as 040 . However, in the powder patterns of the dry samples the 040 and the 220 reflections are separated, and we can see that the 040 reflection contributes most of the intensity at that spacing (the 220 reflection occurs at a slightly smaller spacing in the dry samples). This suggests that the β -sheets are connected along the \mathbf{b} -axis through side-chain contacts, spanning a distance of 9.85 \AA per monomer in the \mathbf{b} -direction. There is little ambiguity about the nature of the peptide backbone structure viewed perpendicular to the \mathbf{c} -axis, since it is the regularly hydrogen-bonded Pauling-Corey parallel β -sheet. The strongest reflection in both the electron diffraction and in the X-ray powder patterns occurs at 4.72 \AA . From the electron diffraction data, we identified this reflection as the 021 . In our model, this reflection arises from the contacts made by the amide groups of the side-chains, which are forming ladders similar to those observed for polyglutamine specimens (Perutz, 1999). The arrangement of the peptide monomers in the unit cell is suggestive of a pair of protofilaments, in which a protofilament consists of one of the pairs of β -sheets, which would form a spiral with a pitch of 4.86 \AA , a width of $\sim 30 \text{ \AA}$ and a thickness $\sim 20 \text{ \AA}$, resembling the packing of β -sheets

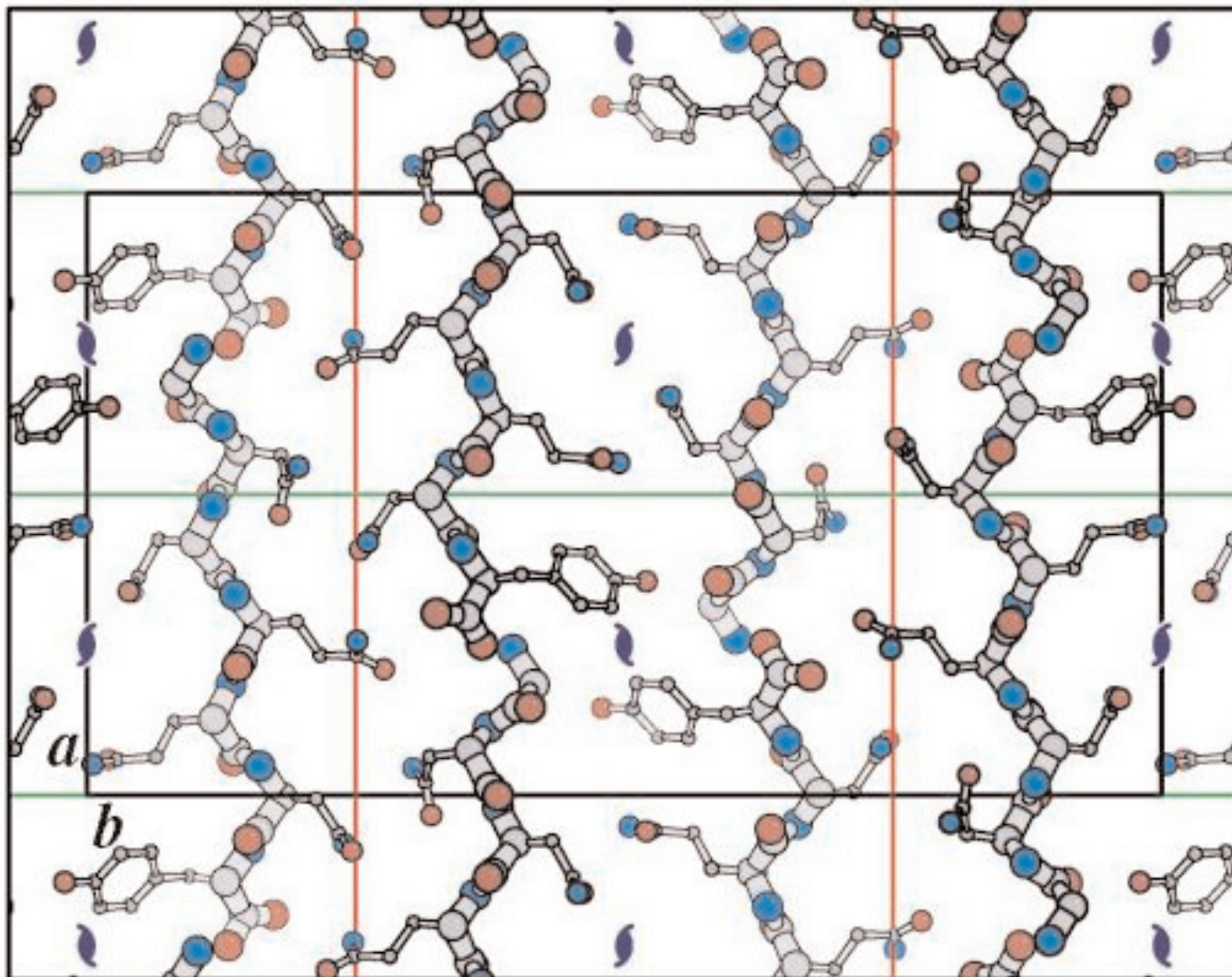


Figure 4. Schematic diagram of the packing of the peptide in the crystals, viewed along the *c*-axis. The presence of $P2_12_12_1$ symmetry implies four peptide molecules per unit cell. The peptide backbone in this model is slightly tilted from the *a*-axis, and the tyrosine's are in close contact due to the presence of a 2-fold screw axis along *c*.

in pectate lyase (Yoder *et al.*, 1993).

The diffraction spots are slightly thinner in the meridional direction ($\sim 1/100\text{\AA}$) than in the equatorial ($\sim 1/80\text{\AA}$), indicating that the correlation length is larger in the *c*-direction than in the *ab*-plane. In the azimuthal direction we observe a half width $\sim 1/140\text{\AA}$. The measurement in the azimuthal direction is independent of artifacts of the CCD detector used for the electrons. We found the width of the spots at half maximum to be variable and not clearly correlated with the intensity of the spot, or its corresponding spatial frequency. The shape of the spots might be perturbed by the presence of inelastic scattering (Spence, 1993).

One of the most interesting properties of this peptide, is the fact that it has eluded all efforts to produce large crystals suitable for single crystal X-ray

crystallography. A tendency to form crystals of limited size might be an inherent property of the β -sheet packing, since β -sheets have a natural tendency to curve, and therefore being in an extended conformation might introduce a cumulative strain that hampers the growth of large crystals, as observed for the crystals of sickle cell hemoglobin (Mu *et al.*, 1998)

The use of electron scattering data for *ab initio* structure analysis has several potential pitfalls, such as dynamical scattering, secondary scattering and crystal bending (Dorset, 1995). However, all the information that we need to see the packing of the peptide in the crystal is contained in the *hk0* reflections, since in the *c*-direction the structure connected in a predictable manner by hydrogen bonds. We have collected electron diffraction intensities that sample the *hk0* plane to $\sim 2\text{\AA}$, but

some of the reflections show non-trivial departures from Friedel's symmetry, indicating a perturbation on the data. Therefore more experiments are needed to ensure that the observed intensities are self-consistent.

Density measurements (Balbirnie *et al.*, 2001) show that the peptide occupies 93% of the volume in the unit cell, which translates to ~2.5 to 3.5 water molecules per peptide. However, calculations of the molecular volumes using the typically observed volumes for Gly, Asn, Gln and Tyr in protein crystals (Tsai *et al.*, 1999), give a peptide volume between 915 and 936 Å³ [3], and consequently, between 4.5 and 5.5 water molecules per peptide in the unit cell. This discrepancy suggests that the side chains in the peptide are forming hydrogen bonds directly with the side chains from the neighboring peptide, largely excluding water in the process. A relatively large activation energy would be required to disrupt this network of hydrogen bonds, pointing to a possible explanation of the stability of the cross-β structures.

Acknowledgements

We would like to acknowledge the help from Drs. Ken Downing and Huilin Li for making the facilities at the LBL available to us, as well as for helpful discussions. This work was supported by NIH grant NS 42221 to D.L.D. Caspar.

References

- [1] Adrian, M., Dubochet, J., Lepault, J. & McDowell, A.W. (1984). Cryo-electron microscopy of viruses. *Nature* **308**, 32-36.
- [2] Astbury, W.T., Dickinson, S. & Bailey, K. (1935). The X-ray interpretation of denaturation of the seed globulins. *Biochem. J.* **29**, 2351-2360.
- [3] Balbirnie, M., Grothe R. & Eisenberg, D.S. (2001). An amyloid-forming peptide from the yeast prion Sup35 reveals a dehydrated β-sheet structure for amyloid. *Proc. Natl. Acad. Sci.* **98**, 2375-2380.
- [4] Benzinger, T.L.S., Gregory, D.M., Burkoth, T.S., Miller-Auer, H., Lynn, D.G., Botto, R.E. & Meredith, S.C. (1998). Propagating structure of Alzheimer's β-amyloid (10-35) is parallel β-sheet with residues in exact register. *Proc. Natl. Acad. Sci.* **95**, 13407-13412.
- [5] Bonnar, I., Cohen, A.S. & Skinner, M. (1969). Characterization of the amyloid fibril as a cross-β protein. *Proc. Soc. Exp. Biol. Med.* **131**, 1373-1375.
- [6] Dorset, D. (1995). *Structural electron crystallography*. Plenum Press, New York.
- [7] Dimmeler, E. & Schroeder, R.R. (2000). Global least-squares determination of Eulerian angles from single electron diffraction patterns of tilted crystals. *J. Appl. Cryst.* **33**, 1088-1101.
- [8] Eannes, E.D. & Glenner, G.G. (1968). X-ray diffraction studies on amyloid filaments, *J. Histochem. Cytochem.* **16**, 673-677.
- [9] Geddes, A.J., Parker, K.D., Atkins, E.D.T. & Brighton, E. (1968). 'cross-β' conformation in proteins. *J. Mol. Biol.* **32**, 343-358.
- [10] Halverson, K., Fraser, P.E., Kirschner, D.A. & Lansbury, P.T. (1990). Molecular determinants of amyloid deposition in Alzheimer's disease. Conformational studies of synthetic beta-protein fragments. *Biochemistry* **29**, 2639-2644.
- [11] Kirschner, D.A., Inouye, H., Duffy, L.K., Sinclair, A., Lind, M. & Selkoe, D.J. (1987). Synthetic peptide homologous to β-protein from Alzheimer's-disease forms amyloid-like fibrils *in vitro*. *Proc. Natl. Acad. Sci.* **84**, 6953-6957.
- [12] Leslie, A.G.W. (1999). Integration of macromolecular diffraction data. *Acta Cryst.* **D55**, 1696-1702.
- [13] Mu, X.-Q., Makowski, L. & Magdoff-Fairchild, B. (1998). Analysis of the stability of hemoglobin S double strands. *Biophys. J.* **74**, 655-668.
- [14] Otwinowski, Z. & Minor, W. (1996). Processing of X-ray diffraction data collected in oscillation mode. *Methods in Enzymology* **276**, 307-326.
- [15] Perutz, M. (1999). Glutamine repeats and neurodegenerative diseases: molecular aspects. *TIBS* **24**, 58-63.
- [16] Rudall, K.M. (1952). The proteins of the mammalian epidermis. *Adv. Prot. Chem.* **7**, 253-290.
- [17] Serpell, L.C. & Smith, J.M. (2000). Direct visualisation of the β-sheet structure of synthetic Alzheimer's amyloid. *J. Mol. Biol.* **299**, 225-231.
- [18] Spence, J.C.H. (1993). On the accurate measurement of structure-factor amplitudes and phases from electron diffraction. *Acta Cryst.* **A49**, 231-260.
- [19] Tsai, J., Taylor, R., Chothia, C. & Gerstein, M. (1999). The packing density in proteins: standard radii and volumes, *J. Mol. Biol.* **290**, 253-266.
- [20] Yoder, M.D., Keen, N.T. & Jurnak, F. (1993). New domain motif - the structure of pectate lyase-C, a secreted plant virulence factor. *Science* **260**, 1503-1507.